ORIGINAL RESEARCH

NIR-II-Absorbing NDI Polymer with Superior Penetration Depth for Enhanced Photothermal Therapy Efficiency of Hepatocellular Carcinoma

Bei Li[1,2,]*, Yuting Luo[1,2,]*, Geng Liu[1,2], Maling Gou [iD][3], Lei Feng[1,2], Xiwen Ye[1,2], Jianrong Xu[1,2], Yaotian Fan[1,2], Zhen You [iD][1,2]

[1]Division of Biliary Surgery, Department of General Surgery, West China Hospital, Sichuan University, Chengdu, Sichuan, 610041, People's Republic of China; [2]Research Center for Biliary Diseases, West China Hospital, Sichuan University, Chengdu, Sichuan, 610041, People's Republic of China; [3]Department of Biotherapy, Cancer Center and State Key Laboratory of Biotherapy, West China Hospital, Sichuan University, Chengdu, Sichuan, 610041, People's Republic of China

*These authors contributed equally to this work

Correspondence: Zhen You, Tel/Fax +86 028 85423823, Email youzhen@wchscu.cn

Introduction: Hepatocellular carcinomas (HCC) have a high morbidity and mortality rate, and is difficult to cure and prone to recurrence when it has already developed. Therefore, early detection and efficient treatment of HCC is necessary.
Methods: In this study, we synthesized a novel NDI polymer with uniform size, long-term stability, and high near-infrared two-zone (NIR-II) absorption efficiency, which can greatly enhance the effect of photothermal therapy (PTT) after intravenous injection into Huh-7-tumor bearing mice.
Results: The in vitro and in vivo studies showed that NDI polymer exhibited excellent NIR-guided PTT treatment, and the antitumor effect was approximately 88.5%, with obvious antimetastatic effects.
Conclusion: This study developed an NDI polymer-mediated integrated diagnostic and therapeutic modality for NIR-II fluorescence imaging and photothermal therapy.
**Keywords:** hepatocellular carcinoma, photothermal therapy, NDI polymer, NIR-II imaging

Introduction

Hepatocellular carcinoma is one of the most important diseases threatening human health, and its morbidity and mortality rates are constantly high and on the rise, seriously threatening people's lives and health and causing great pressure on social security.[1] Primary liver cancer mainly includes hepatocellular carcinoma (HCC), Intrahepatic cholangiocarcinoma (ICC), and mixed HCC-ICC, and different classifications have different characteristics in terms of pathogenesis, histology, biology, choice of treatment and prognosis. Among them, hepatocellular carcinoma accounts for 85%-90% of the total number of liver cancer patients.[2]

Early screening and detection of HCC is a top priority in current research. Various techniques can be used to accurately localize tumor lesions and enable further treatment.[3] Currently, the main clinical diagnostic methods are laboratory tests, imaging tests and liver biopsy. Meanwhile, new methods such as triple detection of hepatocellular carcinoma, detection of other tumor markers, combined detection, and liquid biopsy are constantly being proposed and studied.[4]

There are many traditional treatment strategies for HCC, including radical surgical resection, radiotherapy, chemotherapy, and endocrine therapy.[5] However, current conventional tumor treatments are prone to tumor recurrence, which greatly affects postoperative recovery and quality of life. Newer forms of cancer treatment, such as photo-thermal therapy (PTT),[6–9] photodynamic therapy[10,11] and gene therapy,[12] play an important role in the therapy of
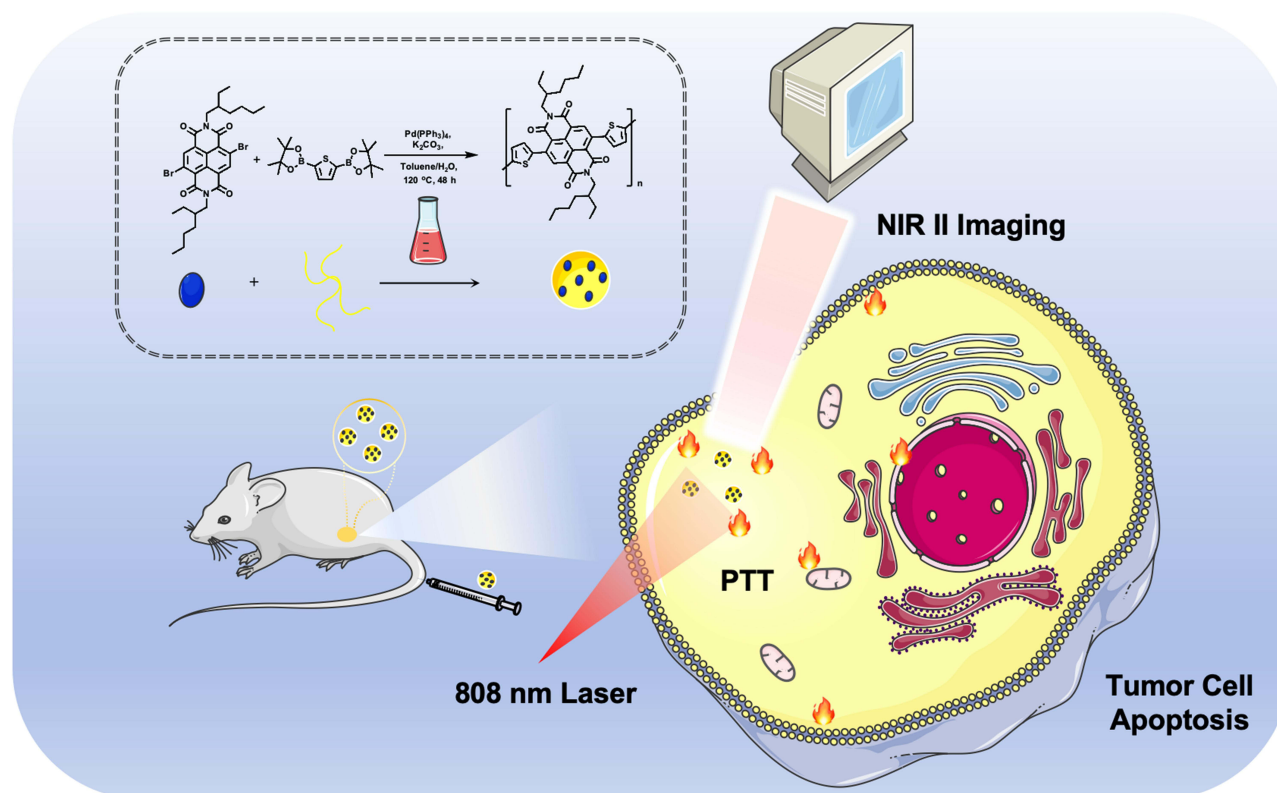
Scheme 1 Schematic illustration of preparation of the novel NIR-II polymer to enhance the tumor penetration and photothermal therapy efficiency for HCC.

HCC.[13,14] PTT has the advantages of high efficiency, low trauma, and high selectivity, all of which are clinically significant. Therefore, NDI polymer can be used as an NIR-II photosensitizer for real-time tracking and guidance to the tumor site and as PTT trigger to kill tumor cells, which has important clinical application prospects in HCC treatment.[15]

Herein, as shown in Scheme 1, we report a novel NDI-based NIR-II fluorescent polymer that enables precise diagnosis and highly efficient treatment of cancer. The designed novel NDI polymers have uniform size, long-term stability, obvious NIR-II fluorescence and high photothermal conversion efficiency. The in vitro NIR-II fluorescence was observed in Huh-7 cells, and in vivo the distribution and tumor enrichment of NDI polymers in Huh-7 tumor-bearing mice were monitored by the NIR-II fluorescence system. Finally, after the NDI polymers were injected into Huh-7 tumor-bearing mice via tail vein, a significant PTT process was carried out on subcutaneous tumors with 808 nm laser irradiation, which efficiently killed the tumors and inhibited the tumor development.

Experimental Section
Materials and Reagents
Naphthalenediimide, thiophene borate, tetraphenylphosphine palladium, potassium carbonate, and dichloromethane were purchased from Aladdin Biochemical Technology Co. Ltd. (Shanghai, China). Ltd. All the cell culture products were supplied by GIBCO (Grand Island, NY, USA). Cell Counting Kit-8 (CCK-8) was obtained from Dojindo Molecular Technologies (Kumamoto, Japan). Crystal violet staining solution was supplied by Shanghai Yuanye Bio-Technology Co., Ltd. Calcein-AM/PI double staining kit was supplied by Beyotime Biotechnology. The annexin V-FITC/PI apoptosis detection kit was supplied by Yeasen Co. (Shanghai, China). Deionized water (18.2 MΩcm^{-1}) was generated using a Millipore Milli-Q purification system and used in all experiments. All chemical reagents were of analytical grade and used without any additional treatment or purification.

Synthesis of NDI Polymer

First, the 64.8 mg naphthalenediimide and 33.6 mg of thiophene borate were dissolved in a mixture of 10 mL of toluene and water (volume ratio = 4: 1), degassed for 20 min, then the 12 mg tetraphenylphosphine palladium and 53 mg potassium carbonate were added in an inert atmosphere at 120°C. After 2 days, the mixture was cooled to room temperature and quenched by adding 10 mL of water. Dichloromethane was used for extraction and rapid column chromatography of the product. A red solution with large polarity was collected from the back, and the target product was obtained by rotary evaporation and drying.

Characterization

The morphology and structure of the synthesized NDI polymer were characterized by transmission electron microscopy (TEM, Tecnai G2 Spirit Biotwin, USA). UV−vis spectra were collected using a UV−vis spectrophotometer (Varian Inc., Palo Alto, CA, USA). The hydrodynamic size and zeta potential were measured using a particle size zeta potential analyzer (Nicomp 380 DLS, USA).

In vitro Photothermal Properties

The photothermal performance of NDI polymer was estimated with a hand-held 808 nm laser, which power density was maintained at 1.0 W/cm^2 in all tests. The volume of NDI polymer dispersion in each test was 1 mL. Temperature changes were recorded using a thermal imaging camera and quantified using Testo IRSoft.[16] For time-dependent photothermal performance, the infrared thermal image of relative temperature was taken under the condition of 808 nm laser (1.0 W/cm^2) irradiating 0.1 mg/mL NDI polymer for different time.[17–19] To assess the photothermal stability, laser on/off cycle assays were carried out, in which the NDI polymer with a concentration of 100 µg/mL was irradiated by laser for 80s (laser on) and naturally cooled down without irradiation for another 160 s (laser off). The on/off cycles were repeated 4 times. Following a previously reported method,[20–22] photothermal conversion efficiency was calculated using Eq.

$$\eta = \frac{hA\left(\Delta T_{max} - \Delta T_{max,PBS}\right)}{I\left(1 - 10^{-A_\lambda}\right)}$$

where η is the photothermal conversion efficiency, h is the heat-transfer coefficient, A is the surface area of the container, T_{max} is the maximum temperature of the NDI polymer, $T_{max,PBS}$ is the maximum temperature of PBS, I is the laser power, and A_λ is the absorbance of the NDI polymer at the wavelength of 808 nm.

Cell Culture

Human HCC (Huh-7 cells) were acquired from the Cell Bank of Cobioer (Nanjing, China). The were cultured in high-glycemic DMEM medium containing 10% FBS, 100 U/mL penicillin and 0.1 mg/mL streptomycin under a humidified atmosphere of 37°C and 5% CO$_2$. Cells in the logarithmic growth phase were used for the in vitro and in vivo experiments. Three sets of parallel experiments were performed for each group of cells in the text to ensure reproducibility of the results. The representative results were selected and presented.

Cytotoxicity Evaluation

The Cell Counting Kit (CCK-8) assay was performed to evaluate the dark toxicity (no laser treatment) and phototoxicity (808 nm laser treatment) of the NDI polymer on HCC cell viability, replying to the changes in the OD450 value. In this study, the cells incubated with PBS were used as control group. 10^4 cells/well of Huh-7 cells were cultured with various concentrations of the NDI polymer (0–400 µg/mL). After co-incubation for 24 h and 48 h, the cells were washed twice with PBS and replaced with 100 µL of fresh cell medium. Next, 100 µL of CCK-8 solution (10%, v/v) in DMEM was added to well and incubated for another 4 h, and a standard CCK-8 assay was used to assess the cell viability by measuring the absorbance of each well at OD 450 nm using a Multiskan SkyHigh system. This calculation was performed using the following equation:[23,24]

$$\text{Cell viability } (\%) = (OD_{450nm}\text{of experimental group})/(OD_{450nm}\text{of control group}) \times 100\%$$

Flow cytometry assays were used to investigate the cytotoxicity of PTT. After the cells were treated with different samples in the absence or presence of 808 nm laser irradiation (1.0 W/cm^2, 5 min) and further incubated overnight, they were stained with Annexin-V FITC and PI to monitor the cell apoptosis rate by flow cytometry.

In addition, calcein-AM/PI assay was used for the live/dead cell staining study of NDI polymer,[25] After different groups of cells underwent a series of treatments, a mixture solution of calcein-AM (2.0 μM) and PI (1.5 μM) in PBS was added to each well, and live cells stained with calcein-AM as green fluorescence and dead cells stained by PI as red fluorescence were observed by CLSM.

Animal

Male BALB/c nude mice (age, approximately 6 weeks; body weight, approximately 20 g) were purchased as Animal model from Henan Experimental Animal Center, China. This study was carried out in accordance with the principles of the basic Declaration and recommendations of the Experimental Animal Ethics Committee of West China Hospital of Sichuan University. The protocol was approved by the Experimental Animal Ethics Committee of West China Hospital of Sichuan University (20,220,221,043). The HCC tumor model was established in BALB/c nude mice by injecting 1×10^6 Huh-7 cells into the right flank of mice. When the average tumor volume reached approximately 100 mm^3, these mice were used for in vivo experiments. Five experimental mice were randomly selected in each group to ensure the reproducibility of the results. And the final representative results were shown in the text.

In vivo NIR-II Fluorescent Imaging

The in vivo biodistribution of the NDI polymer in tumor-bearing nude mice was investigated using in vivo NIR-II fluorescence imaging. The HCC-bearing mice received an intravenous injection of NDI polymer, and images were captured at the indicated time points (pre, 6 h, 12 h, 24 h, and 48 h) using the IVIS spectrum (USA).

In vivo Antitumor Efficacy of NDI Polymer

For the in vivo anticancer efficacy assessment, tumor-bearing mice were randomly divided into four groups, each treated with different treatments as follows: (1) PBS, (2) laser (1 W/cm^2, 5 min), (3) NDI polymer (5 mg/kg), and (4) NDI polymer (5 mg/kg) + laser (1 W/cm^2, 5 min). The tumor volume was measured using a caliper as follows: volume = width^2 × length / 2. Tumor volumes and body weights of the mice were recorded every three days for 15 days. Subsequently, the mice were euthanized, and their major organs (liver, heart, lung, kidney, and spleen) and tumors were excised for hematoxylin and eosin (H&E) staining. TUNEL staining was used to detect apoptosis.[26] CD31 antibody was used to detect the extent of angiogenesis at the tumor site.[27]

Statistical Analyses

Data are expressed as mean ± standard deviation (SD) (n ≥ 3). Prism software was used for statistical significance analysis. The signal indicates a significant difference (*P <0.01, **P <0.005, and ***P <0.001).

Results and Discussion
Synthesis and Characterization of NDI Polymer

As shown in Figure 1A, the NDI polymer composed of 4.9-dibromo-2,7-bis(2-ethylhexyl)benzo[lmn][3,8] phenanthroline-1,3,6,8(2H,7H)-tetraone (NDI-2Br) was synthesized using 2.5-bis(4,4,5,5-tetramethyl-1,3, 2-Dioxaborolan 2-yl)thiophene (Tp-2Bpin) via a catalytic process. The specific synthesis process of the naphthalene diimide raw materials was based on the literature,[28] and the product was confirmed by nuclear magnetic resonance hydrogen spectroscopy (Figure S1). The GPC data of the target product NDI polymer showed that its Mn was 1523, Mw was 2350, and molecular weight was small, indicating that the polymer had a low polymerization degree and belonged to an oligomer (Figure S2). The infrared spectrum shows that the peak of NDI-2Br at 720 cm^{-1} corresponds to the stretching vibration of C-Br. The peak of Tp-2Bpin at 690 cm^{-1} belongs to the stretching vibration peak of C-B, and the two peaks disappear for the oligomers after the reaction, which proves that the two functional groups react accordingly. In addition, the peaks at 1690 cm^{-1} for
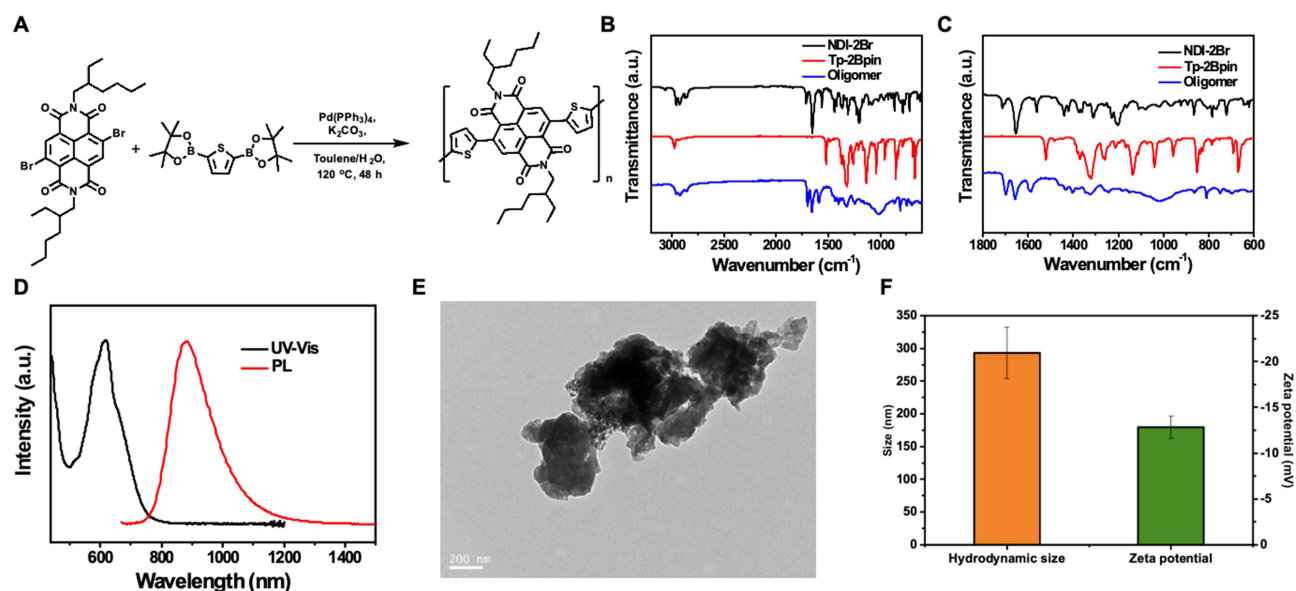
Figure 1 Synthesis and characterization of NDI polymer. (**A**) The illustration of the synthesis of NDI polymer. (**B** and **C**) FTIR vibration spectra for NDI-2Br, Tp-2Bin and NDI polymer Oligomer. (**D**) UV-Vis spectra and fluorescence spectra of NDI polymer in the range of 400–1500 nm. (**E**) TEM imaging of NDI polymer. Scale bar, 200 nm. (**F**) DLS size and Zeta potential of NDI polymer (mean ± standard deviation (SD), n = 3).

naphthalimide raw materials and oligomers belonged to the C=O stretching vibration peak of naphthalimide, and the peaks at 1320 cm^{-1} for thiazole borate Tp-2Bpin and oligomers belonged to the thiophene ring stretching vibration (Figure 1B and 1C). The presence of these peaks in the oligomers also proves that they are composed of these two units. Thus, the accuracy of this reaction was confirmed. Spectrum-related physical Characterization of oligomers was performed. As shown in Figure 1D, the oligomer has an obvious absorption peak between 500 and 800 nm in toluene, with a maximum absorption peak at 617 nm. In addition, the PL spectrum showed that the fluorescence peak of the oligomer was between 700 nm and 1300 nm, and the maximum peak was near 880 nm. The Stokes shift was 263 nm. Notably, the fluorescence peak has an obvious tail after 1000 nm, which proves that the oligomer can be used for NIR-II fluorescence imaging. In addition, the TEM results in Figure 1E show that the synthesized NDI polymer displays highly uniform sizes, with an average diameter of approximately 270 nm. Corresponding to this, the DLS and Zeta potential results showed that the hydrodynamic size of the NDI polymer was approximately 293.3 nm and its zeta potential was approximately −12.8 mV (Figure 1F).

Photothermal and NIR-II Fluorescence Peculiarity

Moreover, long-term stability was investigated by monitoring the DLS size for 10 days. As shown in Figure 2A, there were no significant DLS size changes in NDI polymer regardless of room temperature or 37°C, demonstrating its high stability in PBS. To further test the stability of the NDI polymer, it was dissolved in PBS and cell culture medium and collected by centrifugation after 2, 4, 6, 8, and 10 days. The DLS size of the NDI polymer was then measured again. The results showed that the particle size of the NDI polymer in the cell culture medium increased slightly to 320 nm. However, the NDI polymer in the cell culture medium exhibited excellent stability within 10 days (Figure 2B). In addition, infrared thermal images were used to evaluate the PTT conversion capability of the NDI polymer under 808 nm laser irradiation. Photographs and relative temperature values were recorded using an infrared thermal-imaging camera (Testo, Germany). As shown in Figures 2C and S3, the initial temperature of the samples was 18.1°C, which the value was consistent with the room temperature. With the prolonging of 808 nm laser irradiation (1.0 W/cm^2, 5 min), the temperature enhancement values (ΔT) of 0.1 mg/mL NDI polymer were 30.7°C. This result is clearly different from the phenomenon of no significant temperature increase with PBS illumination, which could be used for PTT therapy. The photothermal conversion efficiency of the NDI polymer was evaluated. After the 808 nm laser irradiation for 80s, the temperature of 0.5 mg/mL NDI polymer solution can reach more than 70°C, and after the laser was turned off for 120 s (Figures 2D and S4), the suspension was rapidly cooled to
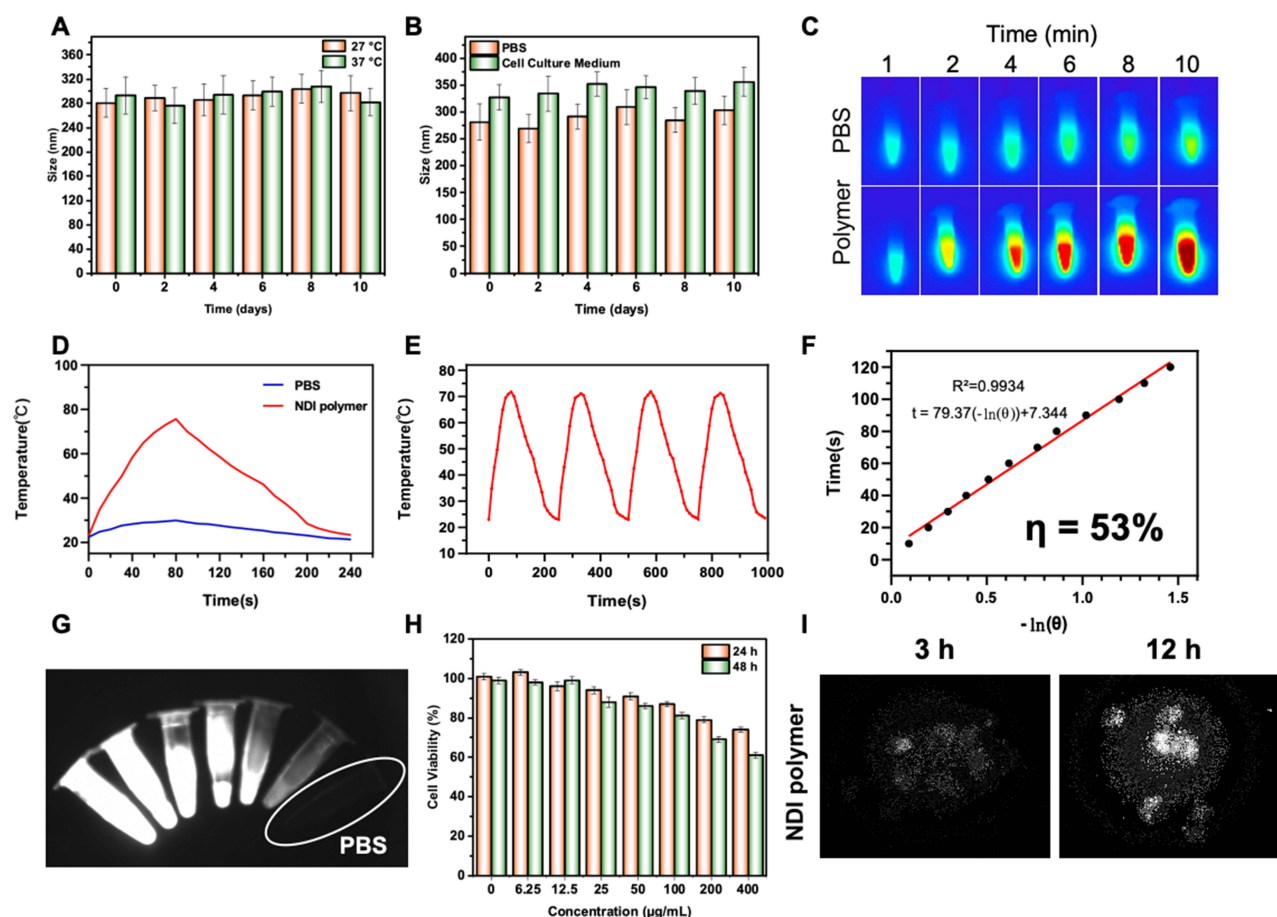
Figure 2 Photothermal and NIR-II fluorescence peculiarity. (**A**) The long-term stability evaluation of NDI polymer over a period of 10 days at 27°C and 37°C, respectively. (**B**) The long-term stability evaluation of NDI polymer over a period of 10 days in PBS and cell culture medium, respectively. (**C**) Infrared thermal images of 0.1 mg/mL NDI polymer solution in the presence of 808 nm laser treatment (1.0 W/cm^2, 5 min). (**D**) Heating and cooling curves of NDI polymer (500 μg/mL) under 808 nm laser irradiation (1.0 W/cm^2). (**E**) Temperature changes of NDI polymer (500 μg/mL) over six laser on/off cycles upon 808 laser irradiation. (**F**) Linear time data versus -lnθ obtained from the cooling period. (**G**) NIR-II fluorescence results of NDI polymer at different concentrations and PBS under 980 nm laser. (**H**) Relative viabilities of Huh-7 cells treated by varied concentrations of NDI polymer (mean ± S.D., n = 3). (**I**) NIR-II fluorescent images of Huh-7 cells after incubated with 50 μg/mL NDI polymer for 3 h and 12 h, respectively.

below the physiological temperature (37°C). These results indicate that the NDI polymer can quickly and efficiently convert light energy into heat energy, which can cause irreversible cell damage at high temperatures. Because poor photostability can greatly limit the therapeutic effect of photothermic agents, six 808 nm laser on/off experiments were conducted to further evaluate the photothermal stability of the NDI polymer. After a 0.5 mg/mL NDI polymer solution was irradiated by an 808 nm laser for 2 min, the laser was turned off immediately to cool the solution naturally for 2 min, and then the above process was repeated. As shown in Figure 2E, the trend of temperature change in each period is relatively consistent, and there is no obvious decrease in the process of temperature increase, indicating that the NDI polymer has good photothermal stability. According to the fitted curve (Figure 2F), the photothermal conversion efficiency (η) of NDI polymer is calculated to be 53%. These results indicated that the synthesized NDI polymer is a highly effective photothermal agent for the photothermal treatment of HCC.

In addition, the NDI polymer exhibits excellent NIR-II fluorescence properties. As shown in Figures 2G and S5, with the excitation of the 980 nm laser, the fluorescence of NIR-II in the NDI polymer was significantly concentration-dependent.[29] From left to right, the concentrations of the NDI polymer were 320, 160, 80, 40, 20, and 10 μg/mL, respectively, and the completely dark tube on the far right represents the PBS group. Prior to detecting the intracellular NIR-II fluorescence effect, the appropriate NDI polymer concentration was determined using the CCK8 assay. As shown in Figure 2H, owing to the excellent biocompatibility of the NDI polymer, no obvious cell death was observed after

incubation with the NDI polymer at various concentrations (0–50 μg/mL) in the dark. They retained a high cell viability about 86.5%, even rich to a concentration of 50 μg/mL, indicating the good biocompatibility of NDI polymer. Huh-7 cells were incubated with NDI polymer solution at 50 μg/mL, and the fluorescence intensity of NIR-II in the cells was observed using a full-spectrum fluorescence microscope. PBS-cultured cells served as controls. As shown in Figures 2I and S6, NDI gradually excited the white NIR-II fluorescence signal after incubation for 3 h, which was significantly different from control group. When the culture time was extended to 12 h, a prominent white NIR-II fluorescence signal was observed. The average signal at 12 h was approximately 2.8 times that at 3h, due of improved cell uptake efficiency. This indicated that the NDI polymer can be fully qualified for the clinical task of NIR-II fluorescence-targeting tracers in vivo.

In vitro Antitumor Effect

To evaluate the therapeutic effect of the NDI polymer photothermal treatment, flow cytometry was performed with an Annexin V-FITC/PI apoptosis detection kit to observe the apoptosis and necrosis ratio of cells induced by different treatments. As shown in Figure 3A, the proportion of normal cells in the PBS control group was 94.8%. However, the results of the single NDI polymer and single laser groups were very close to those of the PBS group, indicating that no induction of cells occurred. In the NDI polymer-mediated photothermal treatment group, the proportion of normal cells decreased to 21.1%, whereas the proportions of early and late apoptotic cells were 9.15% and 69.1%, respectively. These
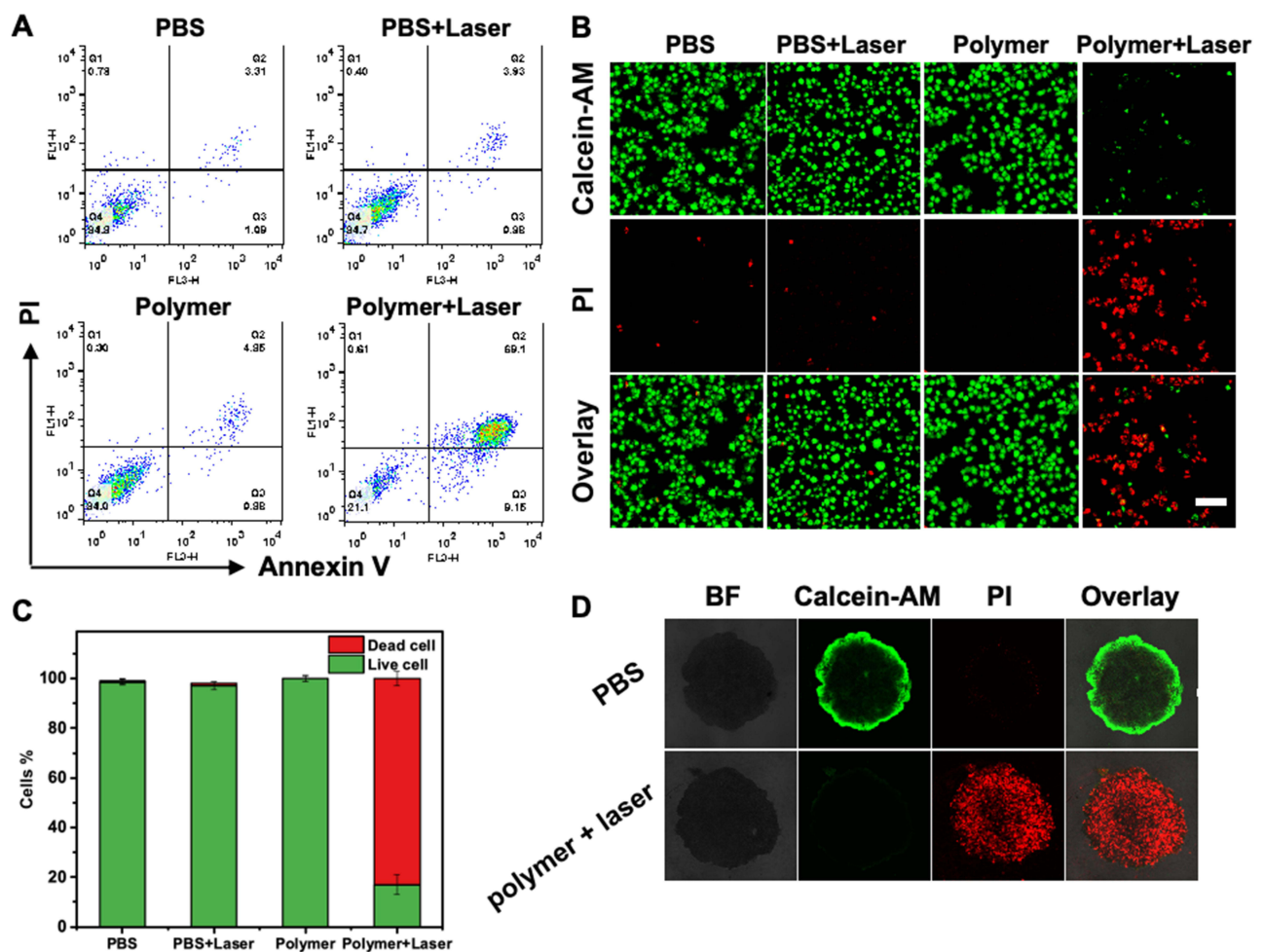

Figure 3 In vitro antitumor evaluation of NDI polymer. (**A**) Apoptosis and necrosis of Huh-7 cells with various treatments (Laser: 1.0 W/cm², 5 min. NDI polymer: 50 μg/mL) analyzed by flow cytometry. (**B**) Live/dead staining of Huh-7 cells with various treatments. Scale bar, 50 μm. (**C**) The relative cellular viability assess recorded from live/dead staining. (**D**) Calcein AM/PI staining images of 3D HCC models after incubated with PBS and NDI polymer under 808 nm laser treatment.

results indicate that NDI polymer-mediated photothermal therapy can induce tumor cell apoptosis to a large extent. To further evaluate the therapeutic effect of NDI polymer-mediated photothermal therapy, calcein-AM/PI double staining was performed. In the fluorescent images, red represents dead cells, and green represents living cells. The results (Figure 3B) show that there were only a small number of dead cells in the PBS, PBS + laser, and NDI polymer groups. However, in the NDI polymer + laser group, a large number of dead cells and only a few living cells were found. According to the semi-quantitative fluorescence analysis (Figure 3C), the proportion of living cells in the first three groups was all higher than 98%, whereas the proportion of dead cells in the NDI polymer + laser group was higher than 80%, which was consistent with the detection result of apoptosis. This indicates that NDI-mediated photothermal therapy has a strong anti-HCC tumor efficacy. In addition, the effect of NDI polymer-mediated photothermal therapy was tested by constructing 3D Huh-7 cell spheres to simulate the internal tumor environment. Finally, the results of calcein-AM/PI double staining (Figure 3D) showed that almost all the live Huh-7 cells in the 3D cell ball of the PBS group were necrotic, whereas most of the Huh-7 cells in the 3D cell ball of the NDI polymer + laser group were necrotic. This phenomenon proves that the NDI polymer can be taken up by the deep part of the tumor to realize global photothermal treatment of HCC tumors.[30]

In vivo NIR-II Fluorescence Imaging

NIR-II fluorescence was used to monitor the drug distribution in the tumor and to indicate the tumor site in vivo. Huh-7 cells were injected subcutaneously into mice for 14 days in advance. When the tumor size reached approximately 100 mm^3, 5 mg/kg NDI polymer was injected through the tail vein, and NIR-II fluorescence imaging was performed 6, 12, 24, and 48 h after injection.[31,32] The results (Figure 4A) showed no fluorescence signal throughout the body of the mice before the injection (pre). From 0 to 24 h after injection, with the gradual accumulation of the NDI polymer at the tumor site, the fluorescence signal of NIR-II gradually increased to the strongest. From 24 h to 48 h, the NIR-II fluorescence signal at the tumor site gradually weakened, indicating that
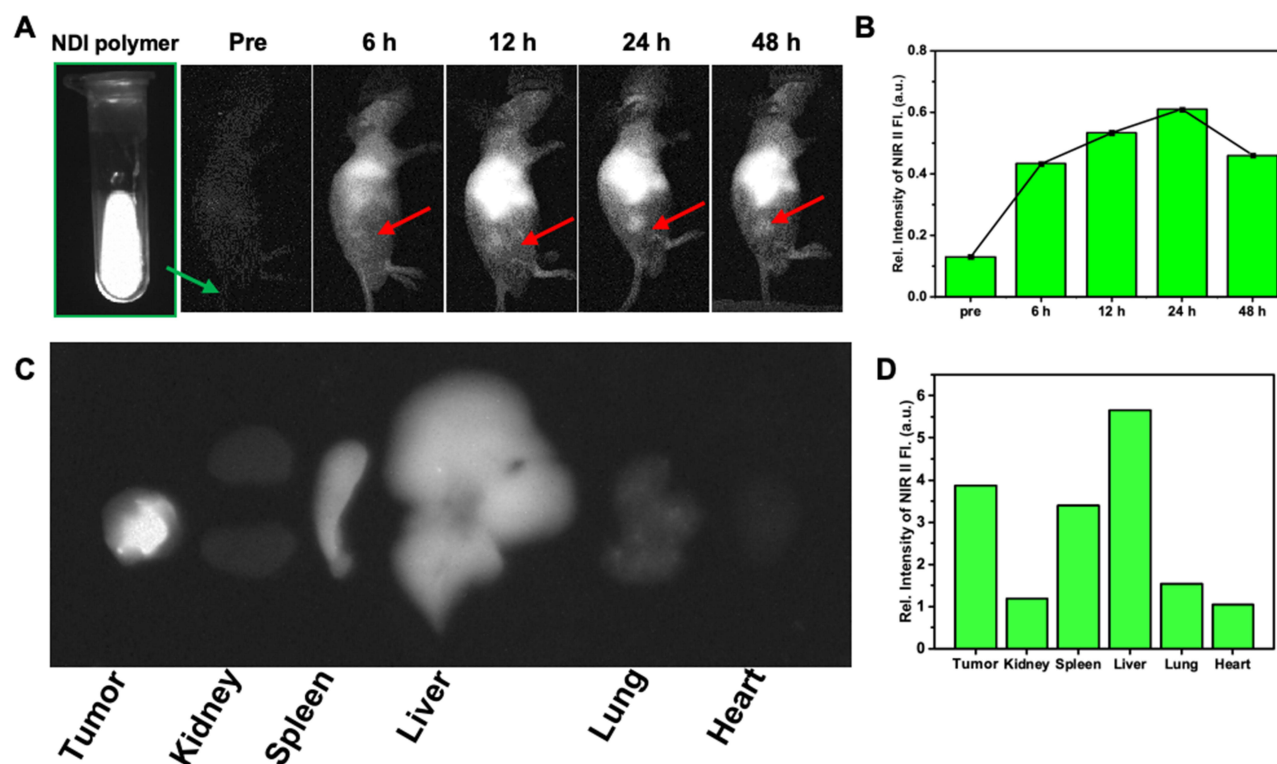

Figure 4 NIR-II fluorescence imaging. (**A** and **B**) Whole-body NIR-II fluorescence images (**A**) and semi-quantitative analysis (**B**) in mice before and after injection of NDI polymer at 6h, 12h, 24h and 48h. The green arrow indicates the injection via the tail vein. The red arrow indicates the location of the tumor. (**C** and **D**) NIR-II fluorescence image (**C**) and semi-quantitative analysis (**D**) of tumor, heart, liver, spleen, lung and kidney.

the NDI polymer began to be metabolized out of the tumor. Experiments have demonstrated that NDI Polymer-mediated NIR-II fluorescence imaging can be used to clinically display tumor sites and monitor drug accumulation at tumor sites in vivo. To be more objective, the NIR-II fluorescence signal intensity of 500 μg/mL NDI polymer under 808 nm laser irradiation of 1.0 W/cm^2 was used as the basis. Semi-quantitative analysis of the NIR-II fluorescence signal in mice before and after the injection of NDI polymer and at different time points (Figure 4B) showed that the signal intensity of the tumor site was only 0.12 before the injection, but the signal intensity increased to 0.43, 6 h after injection, and reached the highest of 0.61 at 24 hours. At 48 h, the intensity decreased to 0.46, which is consistent with the observations. At the same time, we dissected the mice 48 h after the tail vein injection of the NDI polymer and carried out fluorescence intensity detection and semi-quantitative analysis of the tumor and five important organs. The results showed that the NDI polymer mainly accumulated in the liver, tumors, and spleen (Figure 4C and D). NDI polymer aggregation was almost absent in the kidneys, lungs, and the heart.

In vitro Antitumor Effect

NIR-II-guided PTT treatment with the NDI polymer was evaluated in HCC tumor-bearing mice. NDI polymer-mediated photothermal therapy has demonstrated strong tumor inhibition in vivo. As shown in Figure 5A, Huh-7 cells were injected subcutaneously into mice 14 days in advance, and 5 mg/kg NDI polymer was injected into the mice through the tail vein when the tumor size was approximately 100 mm^3. After 1 and 2 days, the tumor was irradiated with an 808 nm laser. The weight and tumor volume of the mice were recorded every three days, and the tumors were analyzed on day 15. A thermal camera was used to observe the photothermal treatment process (Figure 5B),[33] and it was found that the temperature of the tumor site significantly and rapidly increased to 60°C when the 808 nm laser irradiation was performed (0–10 min), whereas the temperature of the tumor site dropped rapidly after the 808 nm laser irradiation was stopped at 12 min, which was close to the normal body surface temperature (Figure 5C). Weight monitoring showed that the weights of the five groups of mice fluctuated within a uniform range (Figure 5D). The monitoring results of the tumor volume of mice (Figure 5E) showed that on the 15th day, the subcutaneous tumors of mice in the PBS group reached more than 800 mm^3, approximately eight times the initial volume. Tumors in the laser and NDI polymer groups also reached more than 700 mm^3, approximately seven times the initial volume. In the NDI polymer + Laser group, the final tumor volume was approximately 50 mm^3, which was reduced by half compared to the initial volume, suggesting that the tumor growth rate significantly slowed or even showed negative growth. This showed that the growth of Huh-7-derived tumors was inhibited in mice, further demonstrating that NDI polymer-mediated photothermal therapy could achieve tumor killing and growth inhibition in vivo. Tumor angiogenesis was also significantly inhibited in the two groups of mice co-treated with NDI polymer and 808 nm laser (Figure 5F), which reflected the ability of NDI polymer-mediated photothermal therapy to inhibit tumor metastasis and invasion in vivo.[34] Terminal deoxynucleotide transferase-mediated dUTP end labeling (TUNEL) images of tumor tissue in the NDI polymer + Laser group showed a more obvious green signal than those in the other three groups (Figure 5F), indicating that NDI polymer-mediated photothermal treatment significantly induced apoptosis in tumor cells.[35] In addition, by comparing the H&E staining results of the five organs of the mice 14 days after the tail vein injection of NDI polymer, it was found that the NDI polymer at 10 mg/kg concentration caused almost no damage to the five important organs of the mice (Figure 5G), which also shows that the NDI polymer has good biocompatibility. In conclusion, the clinical potential of the NDI polymer for the integrated treatment of NIR-II fluorescence and photothermal therapy for HCC tumors in vivo was confirmed.

Conclusions

In this study, we developed an NDI polymer-mediated integrated diagnostic and therapeutic modality for NIR-II fluorescence imaging and photothermal therapy. In the diagnostic process, the NDI polymer efficiently aggregates at the tumor site, and the excited near-infrared II fluorescence can be efficiently separated from the spontaneous infrared light of other tissues in the body, clearly indicating the tumor site and its boundary with the surrounding tissues. Moreover, the excellent photothermal
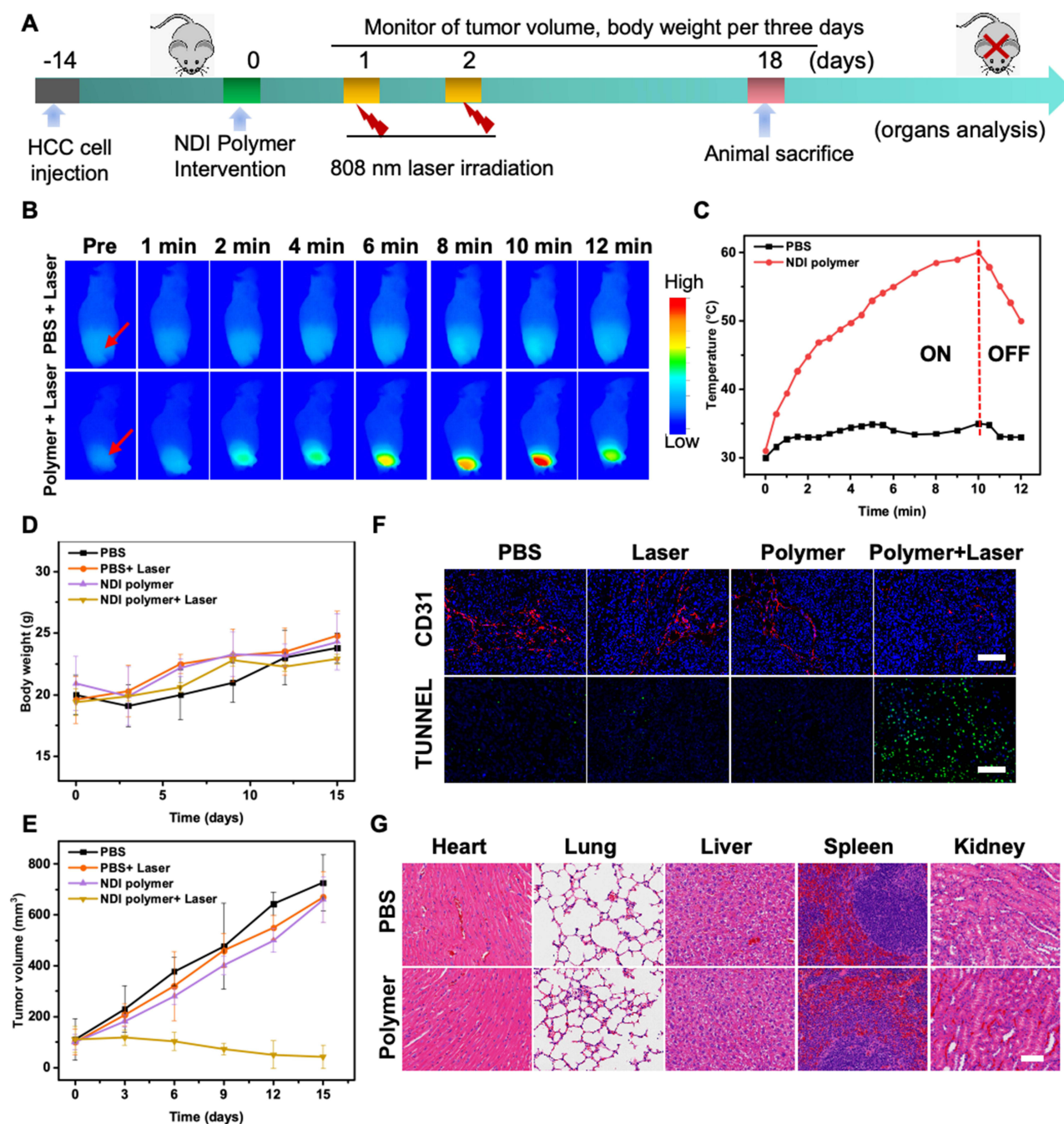
Figure 5 In vivo antitumor evaluation of NDI polymer. (**A**) The schematic diagram of in vivo experiment at HCC tumor-bearing mice. (**B** and **C**) Infrared thermal images of HCC tumor mice and the representative temperature-time changes at the tumor site recorded by infrared thermal device, all the groups (PBS and NDI polymer) with NDI polymer content of 5 mg/kg was intravenous injected into the HCC tumor-bearing mice and monitored the temperature changes after 808 nm laser on (1.0 W/cm^2) or laser off. (**D**) The body weight growth curves of HCC tumor-bearing mice from different groups of 15 days. (**E**) The tumor volume curves of HCC tumor-bearing mice from different groups of 15 days. (**F**) TUNEL-stained and CD31-stained tumor slices in different groups. Scale bar, 100 μm. (**G**) H&E staining images of major organs (heart, lung, liver, kidney and spleen) after intravenous injections of PBS and NDI polymer after 14 days. Scale bar, 50 μm.

conversion efficiency of up to 53% provides NDI polymer with the ability of highly targeted photothermal treatment at the tumor site, which causes HCC tumors lose their activity and metastatic ability by inducing tumor cell apoptosis and killing cancer cells, and ultimately effectively inhibiting the development of tumors. In summary, NDI polymer-mediated integrated diagnosis and treatment has the clinical potential to be a precise treatment strategy for HCC tumors.

Data Sharing Statement

Data supporting the findings of this study are available from the corresponding author upon reasonable request.

Acknowledgments

Disclosure

The authors report no conflicts of interest in this work.

References

1. Llovet JM, Kelley RK, Villanueva A et al. Hepatocellular carcinoma. *Nature Rev Dis Pri*. 2021;7(1):6. doi:10.1038/s41572-020-00240-3
2. Bruix J, Reig M, Sherman M. Evidence-based diagnosis, staging, and treatment of patients with hepatocellular carcinoma. *Gastroenterology*. 2016;150(4):835–853. doi:10.1053/j.gastro.2015.12.041
3. Sangro B, Sarobe P, Hervás-Stubbs S, Ra. M, Melero I. Advances in immunotherapy for hepatocellular carcinoma. *Nat Rev Gastro Hepa*. 2021;18 (8). doi:10.1038/s41575-021-00438-0
4. Yan Q, Sun YS, An R, et al. Application and progress of the detection technologies in hepatocellular carcinoma. *Genes Dis*. 2022;10(5):1857–1869. doi:10.1016/j.gendis.2022.04.003
5. Yang C, Zhang H, Zhang L, Zhu AX, Zhu AX. Evolving therapeutic landscape of advanced hepatocellular carcinoma. *Nat Rev Gastro Hepa*. 2022;1:1.
6. Xingshu L, Lovell JF, Yoon J, Chen X. Clinical development and potential of photothermal and photodynamic therapies for cancer. *Nat Rev Clin Oncol*. 2020;17(11):657–674. doi:10.1038/s41571-020-0410-2
7. Liu Y, Bhattarai P, Dai Z, Chen X. Photothermal therapy and photoacoustic imaging via nanotheranostics in fighting cancer. *Chem Soc Rev*. 2019;48 (7):2053–2108. doi:10.1039/c8cs00618k
8. Xin L, Yong T, Yong T, Yong T, Yong T. Reversing insufficient photothermal therapy-induced tumor relapse and metastasis by regulating cancer-associated fibroblasts. *Nat Commun*. 2022;1:1.
9. Chen Z, Zhao P, Luo Z, Zheng M, Tian H. Cancer Cell Membrane–Biomimetic Nanoparticles for Homologous-Targeting Dual-Modal Imaging and Photothermal Therapy. *ACS nano*. 2016;10(11):10049–10057. doi:10.1021/acsnano.6b04695
10. Yuan Z, Lin C, He Y, Tao B, Chen M. Near-Infrared Light-Triggered Nitric-Oxide-Enhanced Photodynamic Therapy and Low-Temperature Photothermal Therapy for Biofilm Elimination. *ACS nano*. 2020;14(3):3546–3562. doi:10.1021/acsnano.9b09871
11. Zhu L, You Y, Zhu M, et al. Ferritin-hijacking nanoparticles spatiotemporally directing endogenous ferroptosis for synergistic anticancer therapy. *Adv Mater*. 2022;34(51):e2207174. doi:10.1002/adma.202207174
12. Wang D, Tai PWL, Gao G. Adeno-associated virus vector as a platform for gene therapy delivery. *Nat Rev Drug Discov*. 2019;18(5):358–378. doi:10.1038/s41573-019-0012-9
13. Wang J, Meng J, Ran W, et al. Hepatocellular Carcinoma Growth Retardation and PD-1 Blockade Therapy Potentiation with Synthetic High-density Lipoprotein. *Nano Lett*. 2019;19(8):5266–5276. doi:10.1021/acs.nanolett.9b01717
14. Zhou T, Liang X, Wang P, et al. A hepatocellular carcinoma targeting nanostrategy with hypoxia-ameliorating and photothermal abilities that, combined with immunotherapy, inhibits metastasis and recurrence. *ACS Nano*. 2020;14(10):12679–12696. doi:10.1021/acsnano.0c01453
15. Zeng S, Chen J, Gao R, et al. NIR-II photoacoustic imaging-guided oxygen delivery and controlled release improves photodynamic therapy for hepatocellular carcinoma. *Adv Mater*. 2024;36(4):e2308780. doi:10.1002/adma.202308780
16. Cui S, Fan S, Tan H et al, et al. Ultra-homogeneous NIR-II fluorescent self-assembled nanoprobe with AIE properties for photothermal therapy of prostate cancer. *Nanoscale*. 2021;13(37):15569–15575. doi:10.1039/d1nr04227k
17. Zhu Shoujun, Tian Rui, Antaris Alex&er L, Chen Xiaoyuan, Dai Hongjie Near-Infrared-II Molecular Dyes for Cancer Imaging and Surgery Advanced materials. 2019;31:24 e1900321.
18. Hauser D, Estermann M, Milosevic A et al. Polydopamine/Transferrin Hybrid Nanoparticles for Targeted Cell-Killing. *Nanomaterials (Basel)*. 2018;8(12):1065. doi:10.3390/nano8121065
19. Hu Z, Fang C, Li B et al, et al. First-in-human liver-tumour surgery guided by multispectral fluorescence imaging in the visible and near-infrared-I/ II windows. *Nat Biomed Eng*. 2020;4(3):259–271. doi:10.1038/s41551-019-0494-0
20. Xu W, Wang D, Tang BZ NIR-II AIEgens: A Win-Win Integration towards Bioapplications Angew Chem Int Ed Engl, et al. 2021;60:14 7476–7487 doi:10.1002/anie.202005899.
21. Pan X, Lu Y, Fan S et al, et al. Gold Nanocage-Based Multifunctional Nanosensitizers for Programmed Photothermal /Radiation/Chemical Coordinated Therapy Guided by FL/MR/PA Multimodal Imaging. *Int J Nanomedicine*. 2023;18():7237–7255. doi:10.2147/IJN.S436931
22. Yuan M, Liang S, Yan L et al, et al. Rational Design of Platinum–Bismuth Sulfide Schottky Heterostructure for Sonocatalysis-Mediated Hydrogen Therapy. *Adv. Mater*. 2023;35(10):2209589. doi:10.1002/adma.202209589
23. Zhang C, Xin L, Li J et al, et al. Metal-Organic Framework (MOF)-Based Ultrasound-Responsive Dual-Sonosensitizer Nanoplatform for Hypoxic Cancer Therapy. *Adv Healthc Mater*. 2022;11:2 2101946. doi:10.1002/adhm.202101946
24. Zhang S, Jin L, Liu J et al Boosting chemodynamic therapy by the synergistic effect of Co-catalyze and photothermal effect triggered by the second near-infrared light Nano-Micro Letters, et al. 2020;12:1 1–13 doi:10.1007/s40820-020-00516-z.
25. Shan B, Liu H, Li L et al. Near-Infrared II Plasmonic Phototheranostics with Glutathione Depletion for Multimodal Imaging-Guided Hypoxia-Tolerant Chemodynamic-Photocatalytic-Photothermal Cancer Therapy Triggered by a Single Laser. *Small*. 2022;18(4):2105638. doi:10.1002/smll.202105638
26. Tian HQ, An L, Tian Q et al, et al. Ellagic acid-Fe@BSA nanoparticles for endogenous H2S accelerated Fe (III)/Fe (II) conversion and photothermal synergistically enhanced chemodynamic therapy. *Theranostics*. 2020;10(9):4101–4115. doi:10.7150/thno.41882

27. Ruan J, Liu H, Chen B et al, et al. Interfacially Engineered Zn x Mn1–x S@ Polydopamine Hollow Nanospheres for Glutathione Depleting Photothermally Enhanced Chemodynamic Therapy. *ACS Nano*. 2021;15(7):11428–11440. doi:10.1021/acsnano.1c01077

28. He T, Jian C, He J et al, et al. Manganese-dioxide-coating-instructed plasmonic modulation of gold nanorods for activatable duplex-imaging-guided nir-ii photothermal-chemodynamic therapy. *Adv. Mater*. 2021;33(13):e2008540. doi:10.1002/adma.202008540

29. Lin J, Li Y, Wang P et al. Natural Killer Cell Membrane-Cloaked Virus-Mimicking Nanogenerator with NIR-Triggered Shape Reversal and• C/• OH Storm for Synergistic Thermodynamic–Chemodynamic Therapy. *Adv Mater*. 2022;9(5):e2103498. doi:10.1002/advs.202103498

30. Liu G, Zhu J, Guo H et al, et al. Mo2C-derived polyoxometalate for NIR-II photoacoustic imaging-guided chemodynamic/photothermal synergistic therapy. *Angew. Chem. Int. Ed*. 2019;58(51):18641–18646. doi:10.1002/anie.201910815

31. Sun Y, Chen H, Huang Y et al, et al. One-pot synthesis of AuPd@ FexOy nanoagent with the activable Fe species for enhanced chemodynamic-photothermal synergetic therapy. *Biomaterials*. 2021;274():120821. doi:10.1016/j.biomaterials.2021.120821

32. Xiang Q, Yang C, Luo Y et al. Near-infrared II nanoadjuvant-mediated chemodynamic, photodynamic, and photothermal therapy combines immunogenic cell death with PD-L1 blockade to enhance antitumor immunity. *Angew Chem Int Ed Engl*. 2022;18(13):e2107809. doi:10.1002/smll.202107809

33. Qin X, Wu C, Niu D et al, et al. Peroxisome inspired hybrid enzyme nanogels for chemodynamic and photodynamic therapy. *Nat Commun*. 2021;12:1 5243. doi:10.1038/s41467-021-25561-z

34. Zhang H, Li J, Chen Y et al, et al. Magneto-Electrically Enhanced Intracellular Catalysis of FePt-FeC Heterostructures for Chemodynamic Therapy. *Adv. Mater*. 2021;33(17):e2100472. doi:10.1002/adma.202100472

35. Chen Y, Huang Y, Zhou S et al, et al. Tailored chemodynamic nanomedicine improves pancreatic cancer treatment via controllable damaging neoplastic cells and reprogramming tumor microenvironment. *Nano Lett*. 2020;20(9):6780–6790. doi:10.1021/acs.nanolett.0c02622